ACS APPLIED MATERIALS & INTERFACES

Research Article

www.acsami.org

Filling the Voids of Graphene Foam with Graphene "Eggshell" for Improved Lithium-Ion Storage

Bee-Min Goh,[†,∥] Yu Wang,[†,∥] M. V. Reddy,[†] Yuan Li Ding,[‡] Li Lu,[‡] Christopher Bunker,[§] and Kian Ping Loh*[,†]

[†]Department of Chemistry, Graphene Research Centre, National University of Singapore, 3 Science Drive 3, Singapore 117543, Singapore

[‡]Department of Mechanical Engineering, National University of Singapore, 9 Engineering Drive 1, Singapore 117576, Singapore

[§]Air Force Research Laboratory, Propulsion Directorate, Wright-Patterson Air Force Base, Dayton, Ohio 45433, United States

Supporting Information

ABSTRACT: Highly porous, N-doped graphene foam is synthesized by chemical vapor deposition process on nickel foam. The voids of the graphene foam can be filled with curved graphene sheets by impregnating the nickel foam template with micrometer-sized nickel powder. Subsequent etching of nickel produces a graphene "eggshells"-in-graphene foam structure. The reversible capacity of such graphene foam when used as anode in lithium ion battery is improved by the presence of graphene "eggshells", as compared to the unfilled foam. The improvement is attributed to the higher rate of lithium diffusion, better buffering of strain associated with lithiation/delithiation and higher volumetric energy density of the unique eggshell-in-graphene foam structure.

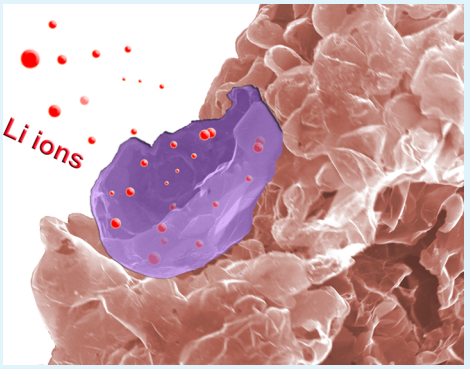

KEYWORDS: *CVD, graphene, lithium ion battery, electrochemistry, capacity*

1. INTRODUCTION

The current lithium ion batteries (LIB) are considered to be one of the most practical solutions to the rapidly growing demand for energy.[1−3] Large-scale energy applications in electric grids, defense, aerospace, transportation, and small portable devices drive the demand for high-performance electrode materials with the capability to store and deliver more energy efficiently.[4] The electrode reaction in a rechargeable lithium battery relies on the simultaneous intercalation of Li^+ and e^- into the active intercalation host.[5] While the shape of the voltage profile and the intrinsic storage capacity are determined by thermodynamic properties of the intercalation host, the rate with which a lithium battery can be charged and discharged depends on kinetic properties such as Li ion mobility and phase transformation mechanism. In the conventional intercalation compounds, the self-diffusion coefficient (D) of Li ion described by the Einstein−Smoluchowski diffusion equation is expressed as follows:[6]

$$D = \frac{\lambda^2 k_B T}{4h} \exp\left(-\frac{\Delta E_{diff}}{k_B T}\right) \quad (1)$$

where h, k_B, and T are Planck's constant, Boltzmann constant and temperature, respectively; λ and E_{diff} denote the diffusion length and diffusion barrier of Li^+ in intercalation compound based on transition state theory.[7] Any variation of the chemical diffusion coefficient D with Li concentration therefore arises from a dependence of the diffusion barrier and vibrational prefactors on the average Li concentration. Due to the exponential dependence of D on ΔE_{diff}, a small variation in the diffusion barrier due to compositional, chemical, or crystallographic changes translates into a large change in the diffusion coefficient, especially at room temperature. As such, there is a need for nanostructured material that can support fast lithium diffusion and accommodate the strain associated with lithium intercalation.[8,9]

Carbonaceous materials, especially graphite, are the most widely employed negative electrode for commercial lithium batteries on account of its low cost, long lifespan, nontoxicity, and high safety record.[10,11] However, the theoretical capacity of graphite is only 372 mAh/g. Strategies used to boost the power capability of electrode materials for Li-ion batteries generally involve reducing the domain size of the active charge-storage material in the electrode to shorten the ion diffusion paths. Nanostructures are particularly attractive in providing fast kinetics.[12] Graphene, as the fundamental building blocks of graphite, has been widely used in energy-related applications.[13,14] It has been touted as possible candidates to improve the performance of LIB due to its high surface area, extraordinary in-plane electrical conductivity, excellent tensile

Received: April 14, 2014
Accepted: May 23, 2014
Published: May 23, 2014

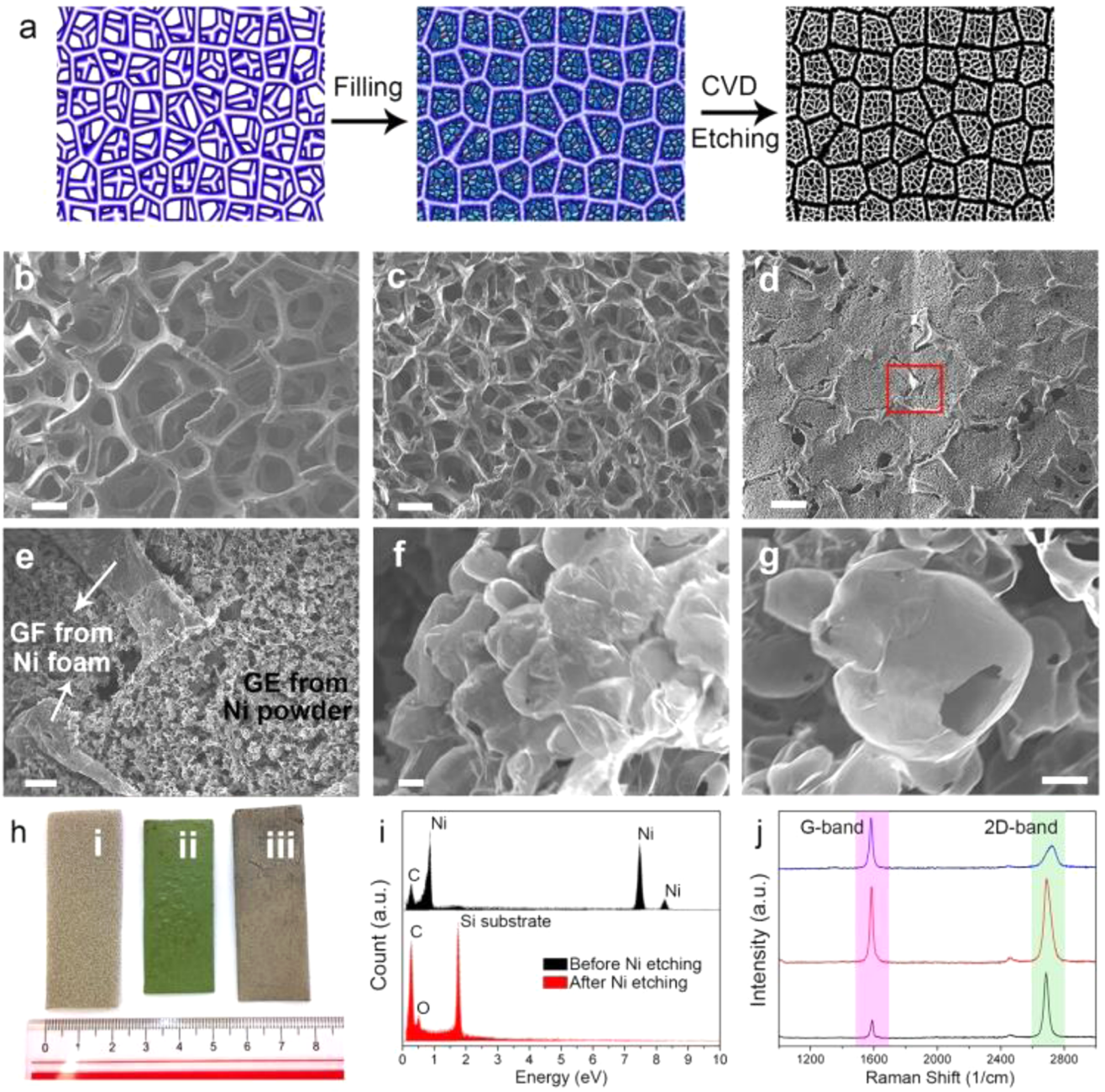

Figure 1. (a) Schematic illustration of the graphene eggshell-filled graphene foam (GE@GF); (b, c) SEM images of graphene foam before and after Ni etching (scale bar = 200 μm). (d) A typical low-magnification SEM image of the GE@GF structure (scale bar = 200 μm). (e) A maginfied SEM image of the red square in (d) (scale bar = 20 μm). (f, g) graphene eggshell structure with open cavities (scale bar = 1 μm). (h) Optical image of the hybrid structure at the different stages. (i) Ni foam; (ii, iii) As-prepared Ni-powder@Ni foam before and after CVD growth, respectively. (i) Comparison of EDX spectra before and after Ni etching. (j) Raman measurements.

modulus, and mechanical durability.[15,16] When rendered in the nanoporous form similar to graphene foam, the high surface area and free space may buffer the volume swing that occurs during charge/discharge cycling of embedded high-capacity metals or metal oxide materials, thereby minimizing electrode destruction from the associated strain.[12,17] Previous work by Ji et al.[18] and Li et al.[19] have demonstrated that graphene foam impregnated with anode material ($Li_4Ti_5O_{12}$) and cathode material (lithium iron phosphate and $LiFePO_4$) shows high rate capability in LIB. On its own, such foam-like material is known to have low volumetric energy density; thus, a material synthesis strategy that allows porosity and yet maintaining high volumetric energy density is needed.

In this work, we develop a porous network composed of hollow graphene "eggshells" filling three-dimensional (3D) graphene foam. In theory, such a unique carbon nanostructure is expected to manifest greatly improved electrochemical performance because of the integration of several advantageous structure features. First, it can offer a high density of cross-plane ion diffusion channels that facilitate charge transport. Second, it can be better for lithium intercalation at high rates due to the strained hollow egg shell structure. Under biaxial asymmetric strain, it has been calculated that the binding energy of Li to

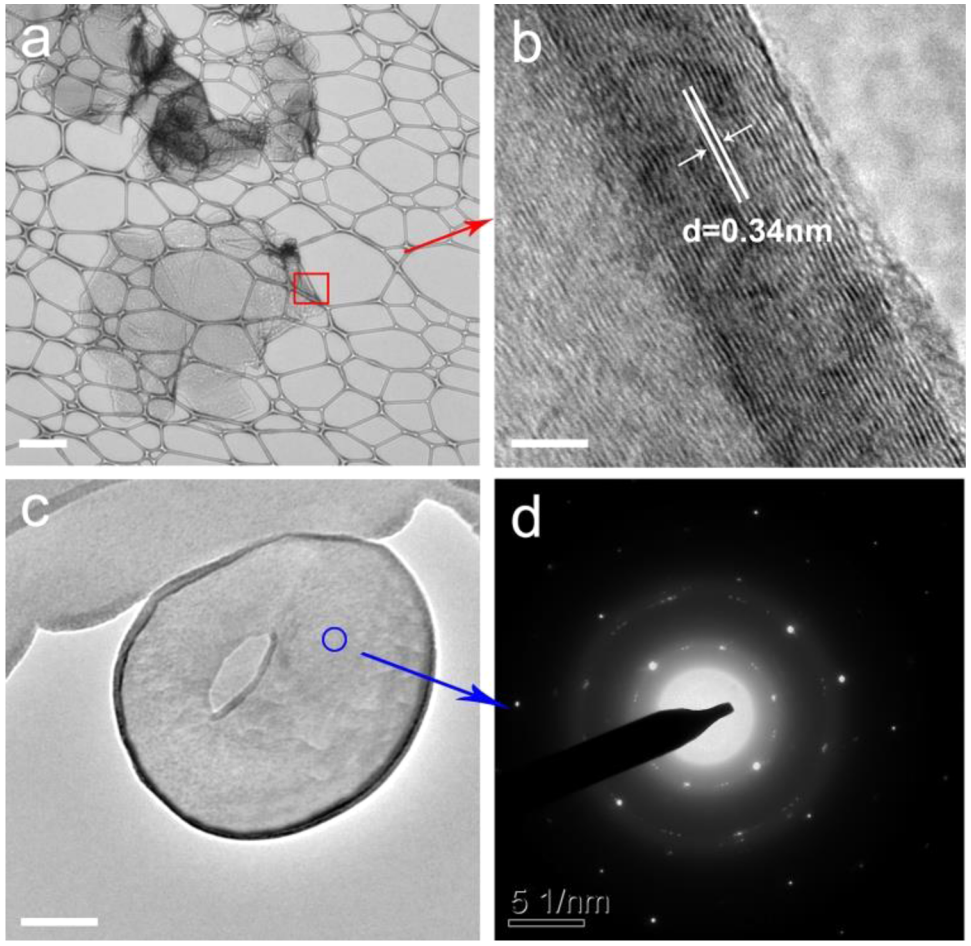

Figure 2. (a, c) TEM images of graphene egg shell structure (scale bar = 500 nm). (b) HRTEM image of the red square in part a, showing crystalline shell wall (scale bar = 2 nm). (d) SAED pattern of the shell wall at the blue circle in part c.

graphene sheet increases by 52% with respect to its bulk's cohesive energy.[20] Third, the hollow structure provides sufficient buffering for volume swing during lithiation and delithiation. At the same time, its multichannels allow fast ionic transport through the electrode during cycling.[21,22] Finally, the in-filling of the 3D graphene foam by the graphene egg shells enhances the volumetric density, electrochemical activity and mechanical stability.[23]

2. EXPERIMENTAL SECTION

The as-synthesized GF and GE@GF electrodes were cut into 16 mm diameter electrodes and dried in oven at 80 °C. The cells were assembled in an argon-filled glovebox with metallic lithium (thickness, Kyokuto metal Co, Japan) as the reference and counter electrode, 1 M $LiPF_6$ in ethylene carbonate (EC)-dimethyl carbonate (DMC) (1:1 volume ratio) as the electrolyte and a glass microfiber (GF/F, Whatman Int. Ltd., Maidstone, England) as the separator. Galvanostatic charge−discharge cycling was carried out on a Bitrode battery tester system (Model SCN-12-4-5/18, U.S.A.) in the voltage range from 3.0 to 0.005 V (versus Li/Li^+). Cyclic voltammetry (CV) was performed on a computer controlled MacPile II unit (Biological, France) at room temperature at a scan rate of 0.058 mVs^{-1} from 0.005 to 3.0 V. Details of electrode fabrication and instrumentation were presented in previous report.[24,25]

3. RESULTS AND DISCUSSION

The synthesis strategy of graphene eggshell-filled graphene foam (denoted as GE@GF) is based on a conventional chemical impregnation method for the preparation of catalyst, followed by chemical vapor deposition (CVD) growth of graphene film and then chemical etching of metal catalyst, as schematically illustrated in Figure 1a (details in Supporting Information). Briefly, an appropriate slurry in viscosity was prepared by mixing Ni powder (2.2−3 μm in diameter) and poly(methyl methacrylate) PMMA (950 PMMA A5, 5% in anisole) under sonication for 30 min. The resulting slurry was well homogenized and was slowly drop-casted into nickel foams (Alantum Advanced Technology Materials (Dalian), ~380g/m^2 in area density, and ~1.2 mm in thichness). The as-prepared PMMA-coated Ni-powder@Ni foam was baked at 80 °C for 5h and then annealed at 200 °C for 10 h. After this, Ni-powder@Ni foam samples were introduced into the furnace for the CVD growth of graphene, where PMMA plays two roles: (1) fixing the Ni powder in Ni foam and (2) provides solid carbon source for the growth of graphene.[26] Figure 1h shows the novel graphene hybrid nanostructure at different stage from Ni foam (i) to Ni-powder@Ni foam (ii) and the one after CVD growth (iii).

In Figure 1b, it can be seen that the Ni foam exhibits a microporous structure with pore sizes ranging from 100 to 400 μm as imaged by Field-Emission Scanning Electron Microscopy (FESEM). After the etching of the Ni foam, the recovered 3D graphene foam shows comparable pore sizes, as shown in Figure 1c. By introducing graphene eggshells into the pores of the graphene foam, the density and mechanical strength of the

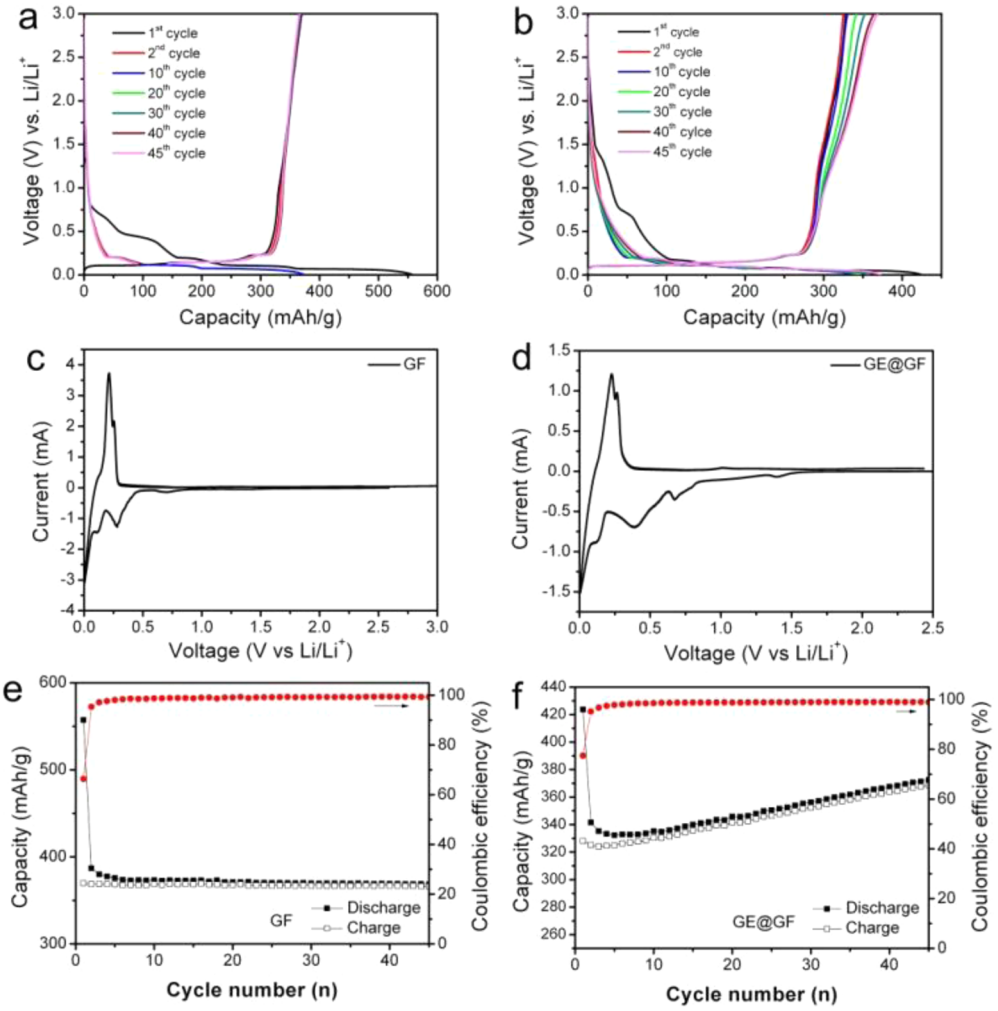

Figure 3. Electrochemical performances of GE@GF and GF. Charge/discharge profiles of (a) GF, (b) GE@GF; cyclic voltammogram of (c) GF, (d) GE@GF; and cycling profile of (e) GF, (f) GE@GF. Galvanostatic cyclings were performed at a current density of 37 mAg^{-1}, voltage = 3.0−0.005 V vs Li/Li^+. Cyclic voltammetry was performed at a scan rate of 58 $\mu V/s$. Red plots indicate the Coulombic efficiencies.

whole hybrid system was dramatically increased, as shown in Figure 1d and e. As shown, the graphene eggshells are packed tightly within the graphene foam (Supporting Information Figure S1), which gives an interconnected electrically conducting network. Meanwhile, the cavity in each graphene eggshell can store Li ions (Figure 1f and g). Energy dispersive X-ray (EDX) analysis (Figure 1i) confirmed the complete removal of Ni powder and Ni foam after the chemical etching. The hybrid GE@GF nanostrucuture was also characterized by Raman spectroscopy (514 nm excitation). Figure 1j show two distinct peaks at ∼1580 cm^{-1} (G-band) and 2705 cm^{-1} (2D-band). One commonly used parameter for judging the layer thickness is the 2D band at 2700 cm^{-1}, which is an overtone of the disorder-induced D band located at 1350 cm^{-1}.[27] The 2D band in monolayer G can be fitted to a single Lorentzian peak, and its full width at half-maximun (fwhm) is ∼30 cm^{-1}, whereas bilayer G can be fitted with four Lorentzian components.[28] With the increase of layer number, the 2D band evolves into a two-peak structure along with a concomitant decrease in intensity with respect to the G band (∼1580 cm^{-1}). On the basis of Raman peak profile analysis, the hybrid GE@GF consists of few-layer graphene (Supporting Information Figure S2).

The detailed structure of GE@GF is further elucidated by high-resolution transmission electron microscopy (HR-TEM) and selected -area electron diffraction (SAED). In agreement with the above SEM findings, a well-defined cavity can be observed inside each microsphere (Figure 2a and c). Figure 2b shows a HRTEM image of the graphene eggshell, where the {002} lattice fringes (3.4 Å) can be clearly observed. The SAED pattern suggests the graphene eggshells are polycrystalline.

Potato-shaped graphite has been reported to have reduced irreversible capacity and high rate performance;[29] hence, we like to find out if the hollow graphene eggshell could achieve the same objectives. Both GF and GE@GF electrodes are subjected to galvanostatic cycling at low current rate of 37 mA g^{-1} in a 1 M $LiPF_6$ electrolyte. The electrochemical performances of the GF and GE@GF are shown in Figure 3. Overall, the cycling profiles of both electrodes resembles that of graphite.[30] During discharge cycle (intercalation), both materials showed a plateau at ∼0.75 V vs Li/Li^+; this is due to the solid electrolyte interface (SEI) caused by the electrolyte decomposition. Another major plateau is observed at ∼0.20 V, which corresponds to Li intercalation. GF electrode delivers the first discharge and reversible capacity at 557 and 370 (±5) mAh g^{-1}, respectively. After 45 cycles, the capacity reaches 366 mAh g^{-1} (Figure 3a). For GE@GF electrode, the first discharge

dx.doi.org/10.1021/am5022655 | ACS Appl. Mater. Interfaces 2014, 6, 9835−9841

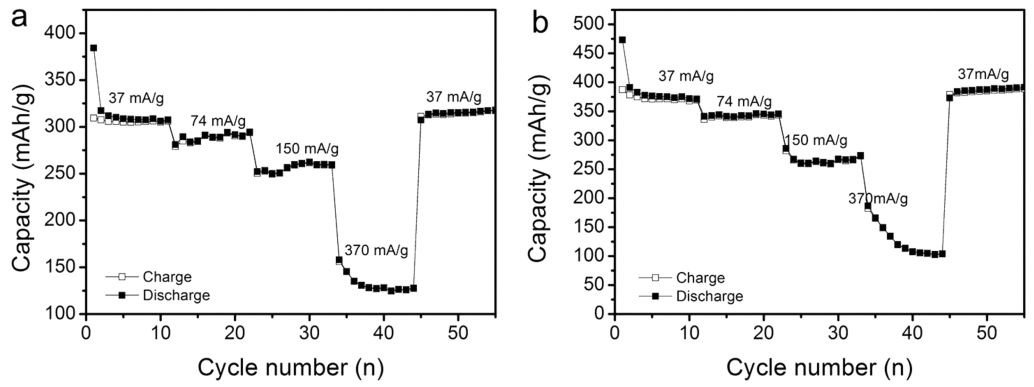

Figure 4. Rate capabilities of (a) GF and (b) GE@GF electrodes over a range of current densities (37 to 370 mA g^{-1}).

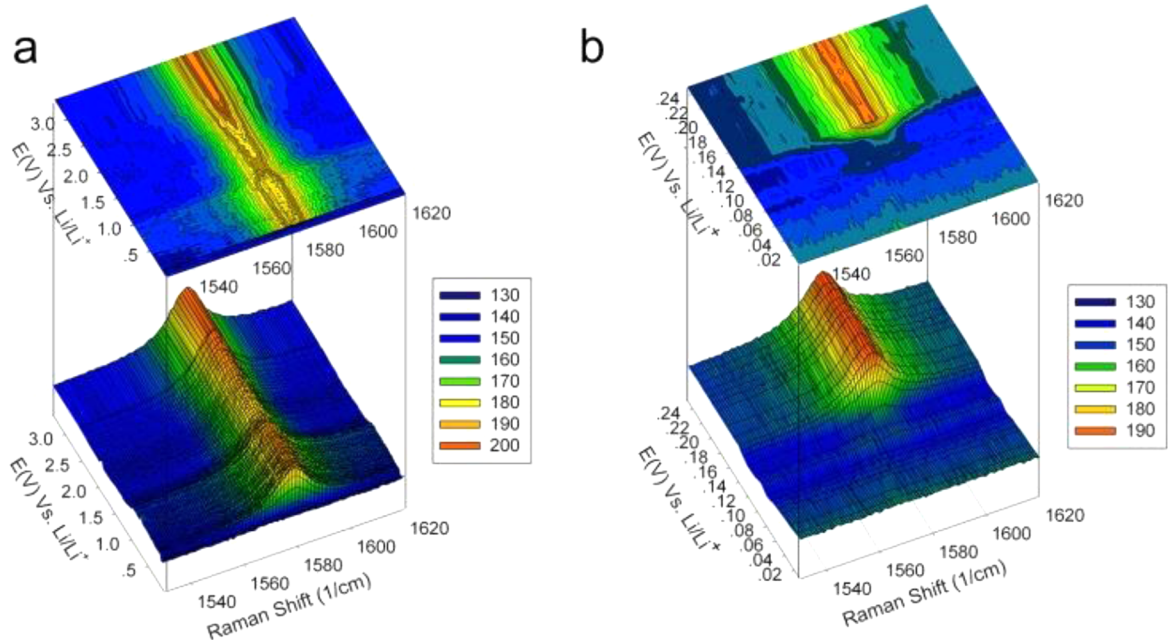

Figure 5. (a) In-situ Raman spectra of GE@GF electrode discharged from 3.0 to 0.005 V vs Li/Li^+. (b) Showing details of part a ranging from 0.25 to 0.005 V vs Li/Li^+.

capacity is 424 mAh g^{-1}, while the reversible capacity achieves 328 mAh g^{-1}. Upon reaching 45 cycles, the capacity increases to 368 mAh g^{-1}, which is comparable to GF electrode (Figure 3b). There are some differences in the galvanostatic curves after the first cycle. At 0.2 V, the GE electrode exhibits flat plateau whereas a hysteretic profile is more prominent for GE@GF electrode. This nonflat plateau suggests the pseudocapacitve storage behavior of the electrode.[19]

The Li storage mechanism of both electrodes can also be studied carefully by slow scanning cyclic voltammetry. Voltammograms of GF and GE@GF in Figure 3c and d depict the reversibility of Li intercalation and deintercalation. The broader curve of GE@GF further reveals capacitive behavior, which may be attributed to the interfacial storage of Li on hollow graphene eggshell.

Parts e and f of Figure 3 show the cycling stability of both electrodes. It is noted that the initial Coulombic efficiency increases from 66.3% for GF to 77.5% for GE@GF electrode. This suggests that the in-filling of the foam by the graphene eggshell reduces the electrolyte decomposition and surface side reaction. The gradual increase in the capacity of GE@GF electrode upon cycling may be attributed to the interconnected graphene eggshell, which enhances the ionic diffusion throughout the graphene network. In addition, with cycling, increasing numbers of active sites and surface defects on the hollow graphene eggshell are activated for Li accommodation. Hence, we surmise that the curvature in the hollow graphene eggshell alters the λ and E_{diff} of Li ion and provides a more efficient intercalation/deintercalation pathway and reduces the initial capacity loss.

LIB with high rate capability is important industrially.[31] The rate capabilities of these two electrodes were tested at current densities from 37 to 370 mA g^{-1} for 10 cycles each as shown in Figures 4a and 4b. The trend of decreasing capacity with higher current densities can be explained by the fact that at high current densities, the ionic motion within an electrode and/or across an electrode/electrolyte interface is not fast enough for charge distribution to reach equilibrium.[32] Nonetheless, the capacity loss is recovered after reducing the rate of charge/discharge. Overall, the GE@GF electrode maintains higher capacity retention than GF electrode. In addition, GE@GF electrode demonstrates good reversibility as its capacity can be restored to ~390 mAh g^{-1} when the current density reduces to the initial value of 37 mA g^{-1}. The better rate performance of

dx.doi.org/10.1021/am5022655 | ACS Appl. Mater. Interfaces 2014, 6, 9835−9841

GE@GF over GF electrode can be attributed to the special structure of the egg- shell graphene. The in-filling of the graphene egg shells increases the volumetric density for Li storage and provides highly accessible thin layers for Li diffusion and intercalation. The graphene eggshell can also flex to accommodate the strain of Li^+ intercalation.[32] All these factors increase the rate of ion transfer between electrolyte and electrodes.[33]

In order to further improve Li storage capacity, we nitrogen-doped the GE@GF electrode using ethylenedieamine as the precursor (details in Supporting Information). It has been shown previously that nitrogen- or boron-doped graphene are capable of enhancing Li ion battery performance in terms of capacity and rate capability.[34,35] Indeed, the storage capacity of N-doped GE@GF is enhanced. It delivers the first discharge capacity of 749 mAh g^{-1} and reversible capacity of 370 mAh g^{-1}. After 45 cycles, the capacity is increased to 459 $mAhg^{-1}$, which is 24.5% higher than pristine GE@GF electrode (see Supporting Information Figure S4). The improved reversible capacity can be attributed to the topological defects on graphene surface caused by the N-doping, leading to a higher electronic conductivity of the active material.[34−36] In addition, N-doped GE@GF electrode shows better rate performance (see Supporting Information Figure S4) as compared to pristine graphene at all current densities. This is due to the improved electrical conductivity and electrochemical activity of doped graphene, which facilitate fast charge and discharge rates.[31]

To obtain further insight into the Li intercalation mechanism of GE@GF electrode, we employed in situ Raman spectroscopy to follow the lithiation process. Figure 5 shows 3-dimensional in situ Raman spectra collected during discharging process of the GE@GF electrode. Overall, it can be observed that G-band shifts gradually to higher wavenumber, and its intensities decrease when it is polarized from 3.0 to 0.005 V vs Li/Li^+. The upshift of G-band indicates the doping effect on graphene where electrons transfer from Li to graphene during intercalation.[37] As evidenced by Figure 5b, G-band intensities weaken upon further polarization and finally disappears at 0.14 V. The disappearance of G-band signifies that Li doping level has reached its maximum level on GE@GF electrode, which causes a reduction in optical skin depth and Raman scattering intensity.[38] This indicates that stage-1 LiC_6 phase has formed on the lithiated GE@GF electrode. This observation agrees with previous finding reported by Pollak et al.[37] and is also verified by our experiments on commercial graphite (see Supporting Information Figure S5).

We also performed ex-situ ^{7}Li Nuclear Magnetic Resonance (NMR) for GE@GF electrode, which was fully discharged to 0.005 V. The NMR spectrum shows the appearance of a peak at 42 ppm, which suggests Li can intercalate into graphene layers of GE@GF electrodes to form stage-1 LiC_6 (Supporting Information Figure S6). This is in good agreement with the observation in graphite electrode as reported by Trease et al.[39]

CONCLUSIONS

In conclusion, we have demonstrated a method to improve the capacity of microporous graphene electrodes by in-filling its cavities with graphene eggshells. The eggshell increases the volumetric energy density and its interconnected networks shorten the Li-ion diffusion pathway and ultimately enhance the rate capabilities. Such morphology control is also effective in improving the initial Coulombic efficiency of the unfilled graphene foam by 17%. Mechanistic study using in situ Raman and ex-situ NMR reveals that the Li intercalation mechanism of GE@GF electrode resembles that of bulk graphite, that is, via stage Li-graphite intercalated compounds, although its overall capacity is higher than that of the theoretical values of graphite. Further work on improving reversible capacity is under way.

ASSOCIATED CONTENT

Supporting Information

Detailed experimental methods, SEM images of graphene eggshells, Raman spectra of the sample, XPS spectra of N-doped GE@GF, electrochemical performance of N-doped GE@GF, and in situ Raman spectra of commercial graphite. This material is available free of charge via the Internet at http://pubs.acs.org.

AUTHOR INFORMATION

Corresponding Author

*Email: chmlohkp@nus.edu.sg.

Author Contributions

‖B.M.G. and Y.W. contributed equally to this work.

Notes

The authors declare no competing financial interest.

ACKNOWLEDGMENTS

This work was supported by a MOE Tier 2 AcRF Grant "Interface engineering of graphene hybrids for energy conversion R-143-000-488-112" as well as AOARD grant 124033 "Fabrication of porous carbon nanostructure for energy storage and transfer application". K.P. Loh also acknowledges provision of NRF-CRP grant "Towards commerical application of grapene R-143-000-546-28". We also thank B. V. R. Chowdari for allowing the use of facilities.

REFERENCES

(1) Scrosati, B. Challenge of Portable Power. *Nature* **1995**, *373*, 557−558.

(2) Tarascon, J.-M.; Armand, M. Issues and Challenges Facing Rechargeable Lithium Batteries. *Nature* **2001**, *414*, 359−367.

(3) Armand, M.; Tarascon, J.-M. Building Better Batteries. *Nature* **2008**, *451*, 652−657.

(4) Dunn, B.; Kamath, H.; Tarascon, J.-M. Electrical Energy Storage for the Grid: A Battery of Choices. *Science* **2011**, *334*, 928−935.

(5) Van Der Ven, A.; Bhattacharya, J.; Belak, A. A. Understanding Li Diffusion in Li-Intercalation Compounds. *Acc. Chem. Res.* **2013**, *46*, 1216−1225.

(6) Chandrasekhar, S. Stochastic Problems in Physics and Astronomy. *Rev. Mod. Phys.* **1943**, *15*, 1−88.

(7) Hänggi, P.; Talkner, P.; Borkovec, M. Reaction-Rate Theory: Fifty Years after Kramers. *Rev. Mod. Phys.* **1990**, *62*, 251−342.

(8) Bruce, P. G.; Scrosati, B.; Tarascon, J. M. Nanomaterials for Rechargeable Lithium Batteries. *Angew. Chem., Int. Ed.* **2008**, *47*, 2930−2946.

(9) Li, J.; Daniel, C.; Wood, D. Materials Processing for Lithium-Ion Batteries. *J. Power Sources* **2011**, *196*, 2452−2460.

(10) Yamaura, J.; Ozaki, Y.; Morita, A.; Ohta, A. High Voltage, Rechargeable Lithium Batteries Using Newly-Developed Carbon for Negative Electrode Material. *J. Power Sources* **1993**, *43*, 233−239.

(11) Tirado, J. L. Inorganic Materials for the Negative Electrode of Lithium-Ion Batteries: State-of-the-Art and Future Prospects. *Mater. Sci. Eng., R* **2003**, *40*, 103−136.

(12) Kaskhedikar, N. A.; Maier, J. Lithium Storage in Carbon Nanostructures. *Adv. Mater.* **2009**, *21*, 2664−2680.

(13) Kou, R.; Shao, Y.; Mei, D.; Nie, Z.; Wang, D.; Wang, C.; Viswanathan, V. V.; Park, S.; Aksay, I. A.; Lin, Y.; Wang, Y.; Liu, J.

Stabilization of Electrocatalytic Metal Nanoparticles at Metal−Metal Oxide−Graphene Triple Junction Points. *J. Am. Chem. Soc.* **2011**, *133*, 2541−2547.
(14) Tong, S. W.; Mishra, N.; Su, C. L.; Nalla, V.; Wu, W.; Ji, W.; Zhang, J.; Chan, Y.; Loh, K. P. High-Performance Hybrid Solar Cell Made from CdSe/CdTe Nanocrystals Supported on Reduced Graphene Oxide and PCDTBT. *Adv. Funct. Mater.* **2014**, *24*, 1904−1910.
(15) Yoo, E. J.; Kim, J.; Hosono, E.; Zhou, H.-S.; Kudo, T.; Honma, I. Large Reversible Li Storage of Graphene Nanosheet Families for Use in Rechargeable Lithium Ion Batteries. *Nano Lett.* **2008**, *8*, 2277−2282.
(16) Liu, J.; Wan, Y.; Liu, W.; Ma, Z.; Ji, S.; Wang, J.; Zhou, Y.; Hodgson, P.; Li, Y. Mild and Cost-Effective Synthesis of Iron Fluoride−Graphene Nanocomposites for High-Rate Li-Ion Battery Cathodes. *J. Mater. Chem. A* **2013**, *1*, 1969−1975.
(17) Chen, D.; Tang, L.; Li, J. Graphene-Based Materials in Electrochemistry. *Chem. Soc. Rev.* **2010**, *39*, 3157−3180.
(18) Ji, H.; Zhang, L.; Pettes, M. T.; Li, H.; Chen, S.; Shi, L.; Piner, R.; Ruoff, R. S. Ultrathin Graphite Foam: A Three-Dimensional Conductive Network for Battery Electrodes. *Nano Lett.* **2012**, *12*, 2446−2451.
(19) Li, N.; Chen, Z.; Ren, W.; Li, F.; Cheng, H. Flexible Graphene-Based Lithium Ion Batteries With Ultrafast Charge and Discharge Rates. *Proc. Natl. Acad. Sci. U.S.A.* **2012**, *109*, 17360−17365.
(20) Hussain, T.; Sarkar, A. D.; Ahuja, R. Strain Induced Li Functionalized Graphane as a High Capacity Hydrogen Storage Material. *Appl. Phys. Lett.* **2012**, *101*, 103907.
(21) Luo, X. W.; Archer, L. A.; Yang, Z. Hollow Micro-/Nanostructures: Synthesis and Applications. *Adv. Mater.* **2008**, *20*, 3987−4019.
(22) Arico, A. S.; Bruce, P.; Scrosati, B.; Tarascon, J. M.; van Schalkwijk, W. Nanostructured Materials for Advanced Energy Conversion and Storage Devices. *Nat. Mater.* **2005**, *4*, 366−377.
(23) Pan, L.; Yu, G.; Zhai, D.; Lee, H. R.; Zhao, W.; Liu, N.; Wang, H.; Tee, B. C.-K.; Shi, Y.; Cui, Y.; Bao, Z. Hierarchical Nanostructured Conducting Polymer Hydrogel with High Electrochemical Activity. *Proc. Natl. Acad. Sci. U.S.A.* **2012**, *109*, 9287−9292.
(24) Reddy, M. V.; Subba Rao, G. V.; Chowdari, B. V. R. Nano-$(V_{1/2}Sb_{1/2}Sn)O_4$: A High Capacity, High Rate Anode Material for Li-Ion Batteries. *J. Mater. Chem.* **2011**, *21*, 10003−10011.
(25) Reddy, M. V.; Yu, C.; Jiahuan, F.; Loh, K. P.; Chowdari, B. V. R. Molten Salt Synthesis and Energy Storage Studies on $CuCo_2O_4$ and $CuO{\cdot}Co_3O_4$. *RSC Adv.* **2012**, *2*, 9619−9625.
(26) Sun, Z.; Yan, Z.; Yao, J.; Beitler, E.; Zhu, Y.; Tour, J. Growth of Graphene from Solid Carbon Sources. *Nature* **2010**, *468*, 549−552.
(27) Malard, L. M.; Pimenta, M. A.; Dresselhaus, G.; Dresselhaus, M. S. Raman Spectroscopy in Graphene. *Phys. Rep.* **2009**, *473*, 51−87.
(28) Ferrari, A. C.; Meyer, J. C.; Scardaci, V.; Casiraghi, C.; Lazzeri, M.; Mauri, F.; Piscanes, S.; Jiang, D.; Novoselov, K. S.; Roth, S.; Geim, A. K. Raman Spectrum of Graphene and Graphene Layers. *Phys. Rev. Lett.* **2006**, *97*, 187401.
(29) Zaghib, K.; Song, X.; Guerfi, A.; Rioux, R.; Kinoshita, K. Purification Process of Natural Graphite as Anode for Li-Ion Batteries: Chemical Versus Thermal. *J. Power Sources* **2003**, *119*, 8−15.
(30) *Lithium Batteries: Science and Technology*; Nazri, G.-A.; Pistoia, G., Eds.; Springer: New York, 2003.
(31) Wu, Z. S.; Ren, W.; Li, F.; Cheng, H. Doped Graphene Sheets as Anode Materials with Superhigh Rate and Large Capacity for Lithium Ion Batteries. *ACS Nano* **2011**, *5*, 5463−5471.
(32) Gowda, S. R.; Pushparaj, V.; Herle, S.; Girishkumar, G.; Gordon, J. G.; Gullapalli, H.; Zhan, X. B.; Ajayan, P. M.; Reddy, A. L. M. Three-Dimensionally Engineered Porous Silicon Electrodes for Li Ion Batteries. *Nano Lett.* **2012**, *12*, 6060−6065.
(33) Xin, S.; Guo, Y. G.; Wan, L. J. Nanocarbon Networks for Advanced Rechargeable Lithium Batteries. *Acc. Chem. Res.* **2012**, *45*, 1759−1769.
(34) Goodenough, J. B.; Kim, Y. Challenges for Rechargeable Li Batteries. *Chem. Mater.* **2009**, *22*, 587−603.
(35) Reddy, A. L. M.; Srivastava, A.; Gowda, S. R.; Gullapalli, H.; Dubey, M.; Ajayan, P. M. Synthesis of Nitrogen-Doped Graphene Films for Lithium Battery Application. *ACS Nano* **2010**, *4*, 6337−6342.
(36) Andersson, A. M.; Abraham, D. P.; Haasch, R.; MacLaren, S.; Liu, J.; Amine, K. J. Surface Characterization of Electrodes from High Power Lithium-Ion Batteries. *J. Electrochem. Soc.* **2002**, *149*, A1358−A1369.
(37) Pollak, E.; Geng, B.; Jeon, K.-J.; Lucas, I. T.; Richardson, T. J.; Wang, F.; Kostecki, R. The Interaction of Li+ with Single-Layer and Few-Layer Graphene. *Nano Lett.* **2009**, *10*, 3386−3393.
(38) Huang, W.; Frech, R. In Situ Roman Studies of Graphite Surface Structures During Lithium Electrochemical Intercalation. *J. Electrochem. Soc.* **1998**, *145*, 765−770.
(39) Trease, N. M.; Koster, T. K.-J.; Grey, C. P. In Situ NMR Studies of Lithium Ion Batteries. *Electrochem. Soc. Interface* **2011**, *20*, 69−73.